JOURNAL OF PROPULSION AND POWER
Vol. 12, No. 5, September–October 1996

Laser Cooling of Neutral Argon for Simulating the Storage of Antimatter

S. Satori,* H. Kuninaka,* and K. Kuriki†
Institute for Space and Astronautical Science, Sagamihara, Kanagawa, Japan

The storage of antimatter in an electrically neutral state is one of the breakthroughs required to realize antimatter applications. In this work, use of laser cooling to manipulate the motion of neutral atoms by radiative pressure was demonstrated using a commercial laser diode and metastable argon as antimatter simulant. The concept of critical velocity was introduced as a criterion for the laser cooling and its importance was experimentally demonstrated.

Nomenclatures

a = acceleration, m/s^2
$\hat{a}$ = normalized acceleration, Hz^2
a_0 = maximum acceleration, m/s^2
$\hat{a}_0$ = normalized maximum acceleration, Hz^2
b = magnetic field, T
$\tilde{b}$ = normalized magnetic field, Hz
b_0 = maximum magnetic field, T
$\tilde{b}_0$ = normalized maximum magnetic field, Hz
$\tilde{C}_0$ = normalized critical velocity, Hz
$f(v)$ = velocity distribution function, dimensionless
h = Planck constant, J s
I = laser-power density, W/m^2
I_0 = saturation power density, W/m^2
k = wave number, m^{-1}
L = deceleration distance, m
M = mass of atom, kg
S_1 = decelerated candidate in velocity distribution function, dimensionless
S_2 = lost candidate in velocity distribution function, dimensionless
$\tilde{v}$ = normalized velocity, Hz
$v(z)$ = velocity, m/s
W = deceleration bandwidth, Hz
z = position, m
$\tilde{z}$ = normalized position, dimensionless
α = constant in Eq. (8), m^{-1} s^{-2}
δ = detuning frequency, Hz
γ = natural linewidth, Hz
λ = laser wavelength, m
μ_e = magnetic moment of electron, J/T

Introduction

ANTIMATTER is an attractive energy source for interstellar space propulsion because of its high energy per unit mass. The interaction between matter and antimatter entirely releases energy several orders of magnitude larger than fusion and fission reactions. As indicated by Forward,[1] on the order of 1-mg antimatter may be required for engineering applications. The number of antiprotons generated by high-energy accelerators has been increasing at the rate of an order of magnitude every 2.5 years.[2] At the beginning of the 1980s, 10-billion antiprotons, or nearly a picogram, could be stored in an accelerator, indicating that applications of antimatter would become realistic early in the 21st century. The expected analytical performance of antimatter propulsion and its application to a wide range of missions[3–6] have been studied since then. Antimatter propulsion is categorized as solid-core type,[7] gas-core type,[8] plasma-core type,[9] pion type,[10] and photon rocket.[11] The pion and photon types are favorable to interstellar missions because of their high specific impulse. The gas core or plasma core rocket is suitable for a near-Earth mission and transportation inside the solar system. In the latter applications, the antimatter is used to heat a propellant gas such as hydrogen that is then exhausted through a magnetic nozzle. Depending on the mission requirements, the thrust and specific impulse of these thrusters can be selected by changing a mixing ratio of antimatter and propellant matter. From an economic point of view,[12] antimatter may become available as fuel for transportation from low Earth orbit (LEO) to geosynchronous orbit (GEO), replacing conventional chemical propellant, if its production cost is reduced to less than 10 million dollars/mg. The price of a milligram of antiproton using present accelerators is 110-billion dollars in the case of Fermi National Laboratory. Theoretically, antiproton cost can be improved by four orders of magnitude if optimized. Since antimatter fuel is extremely expensive, the antiparticles must be carefully handled and preserved so as not to be lost after their generation by accelerator.

The storage of a milligram of antimatter requires tremendous volume if it is in an electrically charged state because of the repulsive coulomb force among particles. For this reason, realistic antiproton storage likely will require neutralization of antiprotons, and will never involve charged antiparticle storage. The stable storage of antimatter in an electrically neutral state will be a key technology for its practical utilization.

The process of antimatter storage is schematically shown in Fig. 1. This conceptual scheme employing the laser cooling was adopted by Forward.[1] The antiprotons generated in the high-energy beam collider are decelerated and are transformed into antihydrogen via recombination with positrons. Once the antihydrogen is formed, it is necessary to manipulate the motion of neutral antiparticles to eliminate any residual kinetic energy. This is done by means of radiative processes. Photon pressure can substitute for current methods employing electrostatic and electromagnetic charged particle traps. The method of antiproton generation has been well studied experimentally[13] and theoretically[14,15] in the field of high-energy physics. While neutral antihydrogen has not been obtained experimentally, the techniques required for its generation have been demonstrated using proton and electron beams.[16] The laser-cooling technique has been recently developed as described later in detail.

Although the collision cross section between photon and particle is in general very small, light of a specific wavelength resonantly interacts with a specific particle in an excited state.

Received Aug. 6, 1994; revision received March 7, 1996; accepted for publication March 31, 1996.

*Research Associate, Space Propulsion, 3-1-1 Yoshinodai. Member AIAA.
†Professor, Space Propulsion, 3-1-1 Yoshinodai. Fellow AIAA.

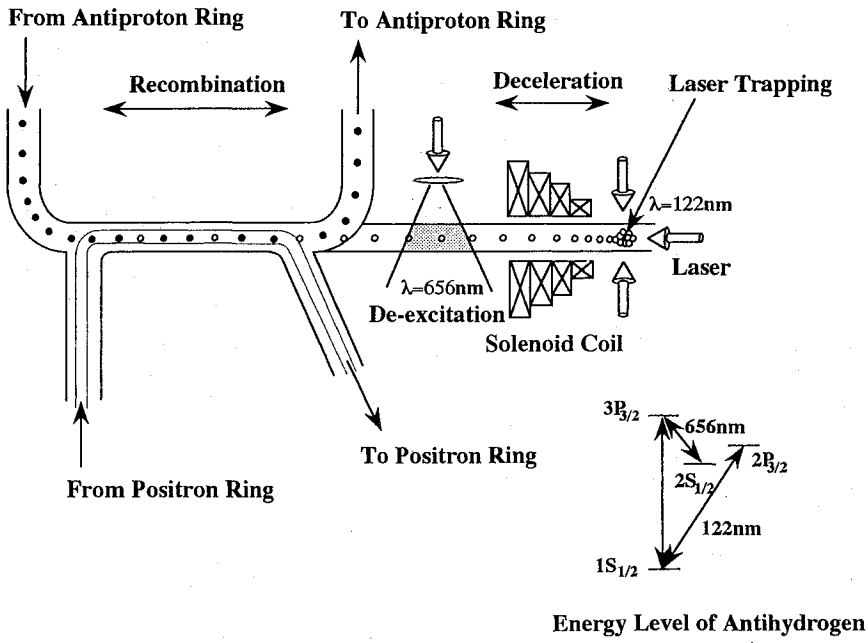

Fig. 1 Antihydrogen breeder.

As discussed, laser cooling is a promising technique for controlling neutral particles. Absorption of a photon tuned to a quantum transition excites the particle to a higher energy level and transfers the photon momentum to the particle. Photon emission associated with the de-excitation is isotropic, resulting in a net momentum change of the particles in the laser beam direction. Laser cooling of sodium has been studied by many authors,[17–20] using the *D* line as the cooling transition. The laser cooling of rare gas highly excited from the ground state was initially performed by Shimizu.[21] Laser diodes as cooling laser were applied to cesium,[22,23] krypton,[24] and argon.[24] Their studies focused on the demonstrations of laser cooling using several atoms, an application to an atomic clock, and a precise measurement of material parameters. Use of laser-cooling techniques for antimatter storage requires that the particle loss mechanisms be investigated in detail because of their economic impacts. Unfortunately, there are few studies focusing on this aspect of laser cooling for neutral particle storage.

This article reports on the experimental study of the final phase of deceleration to simulate neutral storage, replacing the antihydrogen by argon in a metastable state. This substitution is justified on the following grounds. First, it is impossible to obtain and handle antimatter in a conventional laboratory without the use of large accelerators. Second, while current laser technology does not permit the application of laser-cooling techniques to either hydrogen or antihydrogen, ongoing laser technology developments will likely soon permit such applications.[25] However, the fundamental symmetry between matter and antimatter assures the similarity of their behavior during the laser cooling even if argon is used as an antimatter simulant. The lifetime of metastable argon is long enough to assure steady deceleration, since the characteristic time of the order of a millisecond is required for the laser deceleration in a typical laboratory experiment. Our main interest is focused on the investigation of the particle loss mechanisms during the laser-cooling process so that the use of argon has no fundamental effect. Metastable argon has the advantage to use a commercial laser diode of near-infrared wavelength.

The objectives of this article are as follows.

1) Demonstrate the laser cooling of antimatter using argon as simulant.

2) Evaluate the particle loss during laser cooling.

3) Clarify the parametric dependence of particle loss upon the laser intensity and the magnitude and gradient of magnetic field applied along a laser deceleration channel.

Laser Cooling of Metastable Argon

In Fig. 2 the energy level diagram of argon relevant to the diagnostics and the laser cooling is shown. The transition from $1s_5$ to $2p_9$ with a wavelength of 812 nm is used for laser cooling. The laser cooling is based on the Zeeman tuning method with a constant laser frequency. If the excitation–de-excitation cycle between $1s_5$–$2p_9$ repeats many times, the momentum of the atom can be drastically reduced. In the cooling experiment, the laser is introduced in the direction opposite to the atomic beam so that the laser frequency in the moving frame is shifted higher because of the Doppler effect. To compensate for the frequency increment from resonance, an external magnetic field is applied along the cooling chamber. The Zeeman effect then raises the resonant frequency and tunes it to the laser frequency in the moving frame. By decreasing the magnetic field in the direction of the atomic beam, it is possible to continuously compensate for the Doppler shift as the atoms slow down. In the laser-cooling deceleration channel, the magnetic field has a maximum intensity at the entrance of the solenoid coils and decreases gradually to zero at the exit.

Laser-induced fluorescence (LIF) is used to determine the velocity distribution of the atomic beam from the Doppler profile of the $1s_5$–$2p_6$ transition. The drifting atom is excited to the $2p_6$ state absorbing the laser light around 764 nm and emits spontaneous photons of 105 and 108 nm in the de-excitation process to the ground state. The velocity profile of the atomic beam is obtained from the magnitude response of the vacuum ultraviolet (VUV) emission by scanning the diagnostic laser frequency.

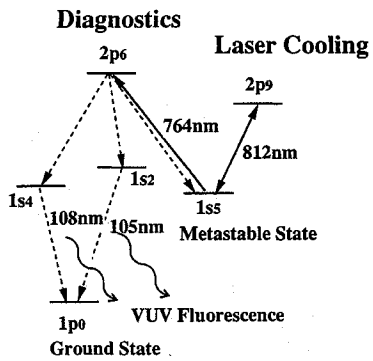

Fig. 2 Energy level diagram of metastable argon.

Experimental Apparatus

The laser-cooling experiment was performed in a high-vacuum environment. In Fig. 3 a top view of the laser-cooling system is shown. The vacuum chamber consists of three sections: 1) the source plasma, 2) the atomic beam extraction, and 3) the laser-cooling sections. Each section is connected to the adjacent chamber through an orifice and the three sections are differentially evacuated by oil diffusion pumps at 10^{-2}, 10^{-3}, and 10^{-5} Pa, respectively. The laser-cooling section is coaxially surrounded by the segmented solenoid coils. Changing the current distribution in the solenoid coils permits control of the distribution of the axial magnetic field intensity in the laser-cooling section. The atomic beam runs from the seed plasma generation section to the cooling section, where the cooling laser is introduced in the opposite direction. An electron multiplier without a shroud (HAMAMATSU R515) to permit VUV emission detection is mounted at the end of the laser-cooling section. The diagnostic laser beam is introduced in the cooling section at an angle of 13 deg to the axis, crossing the atomic beam near the electron multiplier. A part of light split from the diagnostic laser, used as a reference beam for zero Doppler shift, is injected transversely to the beam axis. The diagnostic laser (Sharp LT021) is cooled down to about 200 K by liquid nitrogen in a vacuum environment with a stability range of 1 mK to ensure proper frequency stabilization. The central frequency is swept by slightly changing the driving current of the laser diode. The source plasma containing the metastable atoms is generated in a dc discharge. The collimated beam of excited argon that is extracted through a pinhole has a flux from 9.4×10^7 to 3.1×10^8 cm^{-2} s^{-1}, depending on the mass flow rate, while the beam velocity remains almost constant at a speed of 700 m/s. The argon beam divergence is 5 mrad with a skimmer consisting of a 3-mm pinhole and a 10×10 mm square hole placed 0.62 and 1.85 m downstream from the exit of the plasma source, respectively.

The spectral linewidth and the frequency fluctuation of the cooling laser are required to be of the same order or below the natural linewidth of 6 MHz. Since the typical linewidth of the laser diode is of the order of several tens of megahertz, the longitudinal mode must be actively controlled for laser cooling. An optical feedback method is applied not only to reduce the frequency drift but also to properly select the laser frequency without mode hopping. In Fig. 4 the schematic diagram of the cooling laser is shown. The laser diode (Sharp LT017) is mounted on a Peltier element to keep the temperature fluctuations below 200 μK. The typical power of the laser

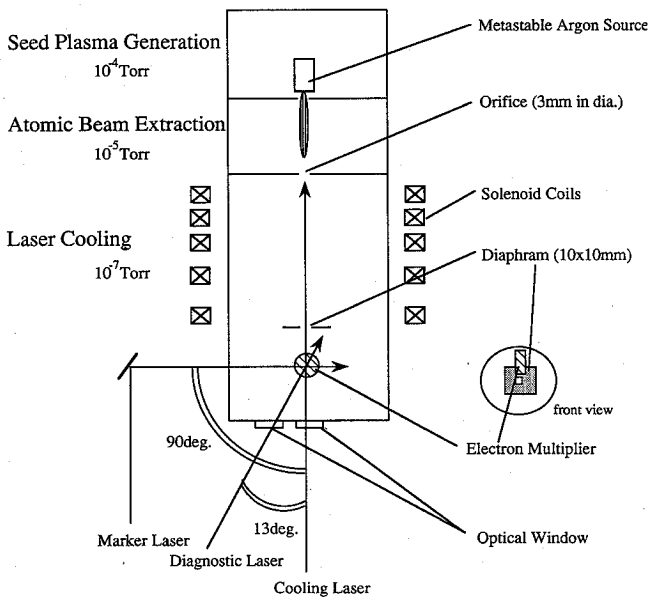

Fig. 3 Geometrical arrangement of laser-cooling experiment.

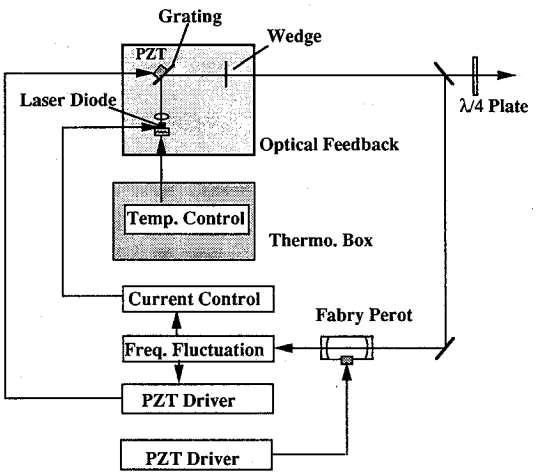

Fig. 4 Block diagram of cooling laser.

was 20 mW. The laser beam is deflected by a grating and 5% of the laser output is reflected back by a wedge placed a distance of 15 cm from the laser diode. The grating is mounted on a piezoelectric transducer (PZT) to control the central frequency precisely, changing the length of the external cavity between the laser and the grating. Measuring the broadening of a saturated absorption signal from the discharge cell by laser-absorption spectroscopy, the linewidth of the laser was roughly estimated to be 10 MHz. To stabilize the laser frequency, the frequency fluctuation is monitored by a confocal Fabry Perot interferometer and the resultant deviation signal is fed back to the PZT voltage and the driving current of the laser. Deviations higher than 1 Hz are fed to the laser current and those lower than 1 Hz are fed to the PZT voltage. The absolute laser frequency was determined by measuring the deviation frequency from the resonance by means of laser absorption spectroscopy with a discharge cell.

Experimental Results

Figures 5a–5c show the typical laser-cooled velocity distribution functions of the atomic beam under the conditions of 7 mW in laser power, 14-mm beam diameter, and 220-G maximum magnetic strength. Each distribution is normalized so that its integrated area should be constant, and the vertical axis is scaled with an arbitrary unit. The horizontal axis denotes the sweep frequency of the diagnostic laser, which will be discussed later. The first peak on the left side in each figure represents the reference laser indicating zero in the velocity distribution function. The frequency of the cooling laser is detuned from the nominal 812-nm light that is resonant to the transition for the rest species. The cooling laser is tuned below the nominal resonant frequency to be tuned with the moving species. In Fig. 5 the laser frequency is indicated by arrows and the resonant frequency is indicated by the origin of the horizontal axis. The absolute values of the detuning frequency and the width of Zeeman shift are denoted in Figs. 5b and 5c. It is found that some atoms are scooped out of the original distribution as seen in Fig. 5a and transferred towards the velocity specified by the detuning frequency. The slowed atoms are accumulated around it. Figure 6 shows the dependence of the peak frequency appearing after the cooling-laser irradiation upon the absolute detuning frequency of the cooling laser. The proportionality observed in Fig. 6 indicates that the peak in the distribution function is identical to the detuning frequency.

To evaluate the efficiency and the parametric dependence of the laser cooling, the decelerated number and recovery factor are defined in Fig. 7, where the distribution of atoms as a function of velocity is shown with the total number of the atoms normalized to unity. Subtracting the postcooled from the precooled distributions, the accumulated number of atoms S_1 and of lost candidates S_2 are obtained. The ratio of S_1 to the

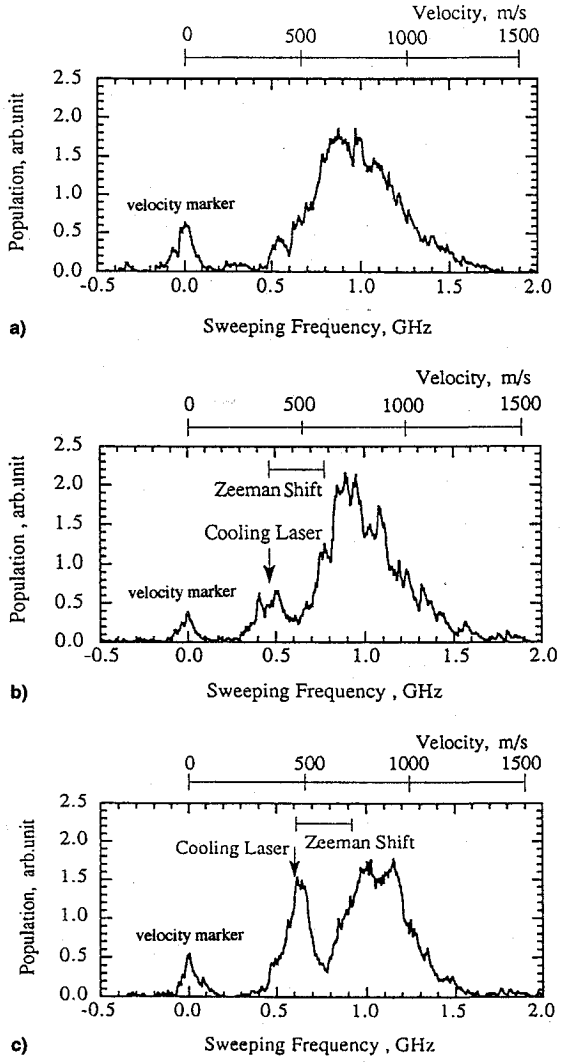

Fig. 5 Velocity profiles of laser-cooled atomic beam: a) without laser irradiation, b) detuning frequency of cooling laser, −440 MHz, and c) detuning frequency of cooling laser, −550 MHz.

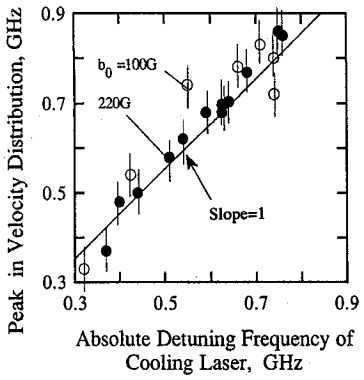

Fig. 6 Relation between absolute detuning frequency of incident laser and peak positions appearing near the detuning point in the atomic velocity space.

integrated area of the distribution, which is set to one, is defined as the decelerated number, and the fraction S_1/S_2 as the recovery factor. For an ideal deceleration, the recovery factor becomes unity because all of the irradiated particles of S_2 are slowed down to S_1. However, in the real experimental condition, this factor is less than unity since the decelerated atoms dissipate transverse to the beam direction because of their thermal motion. This means that the diffusion loss of the particles during laser cooling is reflected in the recovery factor. The decelerated number characterizes the effective decelerated ratio by radiation pressure. The undecelerated candidates, that is, the free-running particles, result in the particle loss. It is preferable for the application to the antimatter storage that both the decelerated number and the recovery factor become as large as possible.

Effect of Magnetic Field Gradient

As shown in Fig. 8, two magnetic field profiles can be generated in the cooling section by changing the current in the solenoid coils. The baseline magnetic field extends over 0.8 m in the beam direction, whereas the steep distribution extends only 0.4 m. Figure 9 shows the decelerated number vs the detuning frequency with the maximum magnetic field strength of 220 G and a laser power of 7 mW. The horizontal axis represents the absolute value of the detuning frequency for the cooling laser. The measurement error is about 30% because of an inevitable ambiguity of the laser spectral linewidth. At an absolute detuning frequency of 0.4 GHz, the deceleration number is about 0.08 with the baseline field geometry and 0.02 with the steep field geometry. The figure shows that the decelerated number of the baseline field is almost always greater than that of the steep field.

Effect of Magnetic Field Strength

Figure 10 shows the relationship between the absolute detuning frequency and the decelerated number for the steep-

$$\text{Decelerated Number} = S_1$$
$$\text{Recovery Factor} = \frac{S_1}{S_2}$$

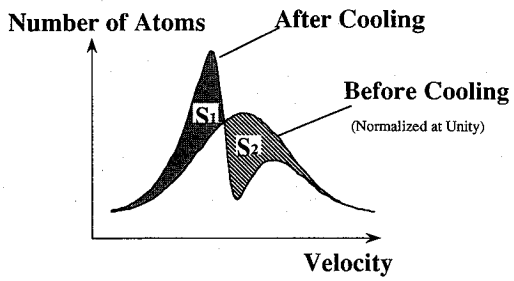

Fig. 7 Definition of decelerated number and recovery factor.

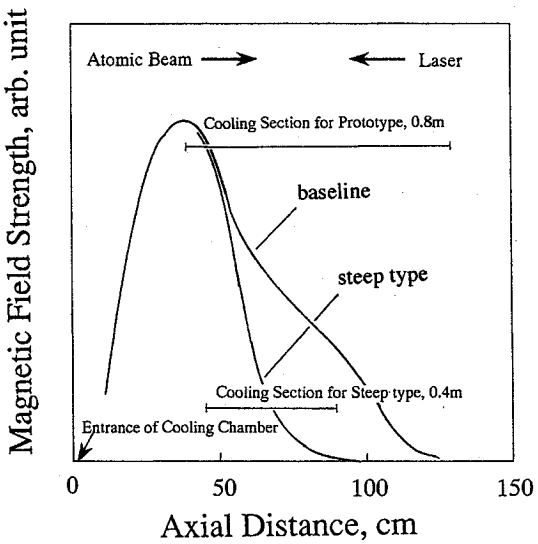

Fig. 8 Field patterns of solenoid coils in deceleration chamber.

type magnetic field with maximum of 100 and 220 G. The curves of calculated results, which will be described in the next section, are also plotted. The maximum decelerated number of 0.12 is obtained at the detuning frequency of −0.85 GHz. The decelerated number increases proportionally to the absolute detuning frequency in the case of a 100-G magnetic field, since, as shown in Fig. 5, the deceleration bandwidth in velocity space shifts toward a more populated region. The decelerated number is inversely affected by the strength of the magnetic field though the corresponding Zeeman shift broadens the deceleration bandwidth. The lower magnetic field value yields more effective deceleration than the 220-G case. Figure 11 presents the recovery factor for the same condition. The recovery factor decreases as the magnetic strength increases and reaches a maximum value of 0.65. A recovery factor less than unity is attributable to the fact that the decelerated particles tend to diffuse out of the beam before entering into the diagnostic area. For the baseline field case the decelerated number also diminishes with increasing magnetic field strength as can be seen in Fig. 12.

Effect of Laser Power

Attenuation of the 7-mW laser power using 0.1 and 0.01 transmittance neutral density filters results in the decelerated numbers shown in Fig. 13, where the maximum magnetic field strength 220 and 400 G were applied and the laser detuning frequency was −0.68 GHz. The decelerated number decreases in accordance with the laser-power reduction because of the

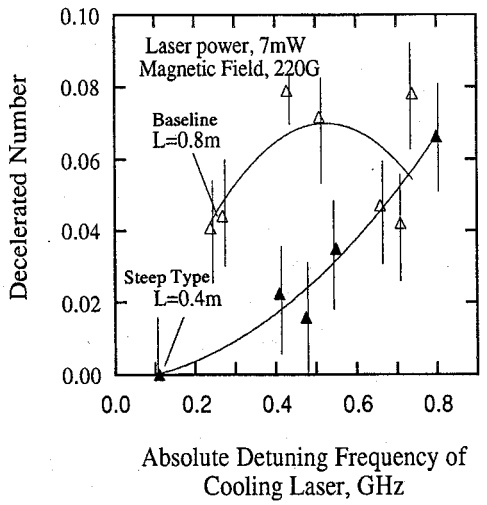

Fig. 9 Dependence of decelerated number on magnetic gradient.

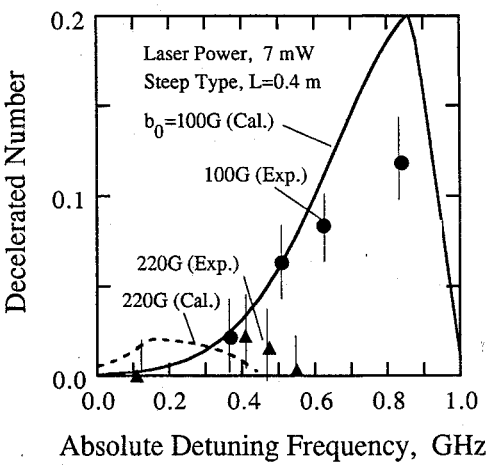

Fig. 10 Dependence of decelerated number on the detuning frequency and the maximum strength of magnetic field.

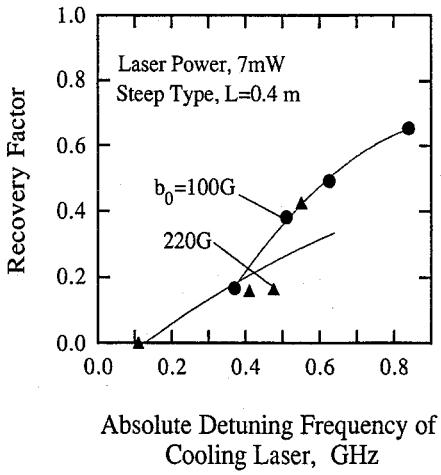

Fig. 11 Dependence of recovery factor on maximum strength of magnetic field.

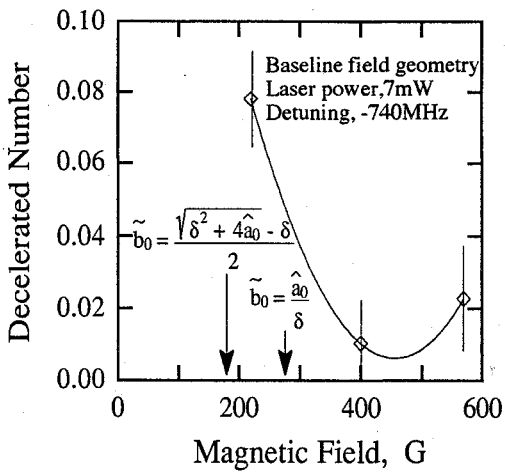

Fig. 12 Relation between decelerated number and magnetic field.

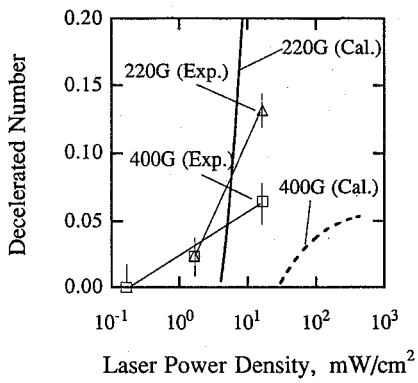

Fig. 13 Dependence of decelerated number on laser power density.

weakening of the radiative pressure. The calculated results are also plotted in Fig. 13.

Discussion

The experimental results show that the decelerated number at a fixed detuning frequency changes depending on the magnetic field strength, the magnetic field gradient, and the laser-power density. The reduction of the decelerated number indicates the appearance of free-running particles, which are not affected by laser though they are tuned to the laser frequency. This implies a particle loss mechanism other than diffusion.

Note that the diffusive loss is likely not serious for either laser cooling or antimatter storage since it can be easily suppressed by adding a transverse cooling.[18]

In this section, we discuss the free-running particle loss mechanism and clarify its parametric dependence. A one-dimensional analysis is used to understand the particle motion in a radiative field. The assumptions are to ignore transverse diffusion caused by statistical fluctuations of numerous spontaneous emissions, and to take the ratio of the natural linewidth of the excited argon atom to the typical Doppler shift to be zero. These assumptions are justified because the diffusive velocity of a few meters per second is very small compared with typical atomic beam velocities of several hundred meters per second, and the typical Doppler shift of about 1 GHz is much larger than the natural linewidth of 6 MHz.

With these assumptions, the acceleration caused by the radiation in an external magnetic field is given by[26]

$$a(z) = \frac{hk\gamma}{2\pi M} \cdot \frac{I/I_0}{1 + I/I_0 + \{kv - 2\pi\delta - [2\pi\mu_e b(z)/h]\}^2/\gamma^2} \tag{1}$$

Taking the limit of zero natural linewidth as assumed previously, Eq. (1) can be approximated as follows:

$$a(z) = \frac{hk\gamma}{2\pi M} \cdot \frac{I/I_0}{1 + I/I_0} \cdot g\left[kv - 2\pi\delta - \frac{2\pi\mu_e b(z)}{h}\right], \quad \frac{\gamma}{kv} \approx 0 \tag{2}$$

where the function $g(x)$ in Eq. (2) represents Dirac's delta function. Equating the argument of the delta function to zero, the equation of motion results. This result can be understood as follows. A particle of given velocity is resonantly decelerated in such a manner that the Zeeman shift completely compensates for the Doppler shift of the atomic beam relative to the cooling laser frequency. The atomic velocity at a point z is given by

$$v(z) = \lambda\{\delta + [\mu_e b(z)/h]\} \tag{3}$$

Differentiating Eq. (3) with respect to z, the radiative acceleration $a(z)$ is obtained as

$$a(z) = -v(z)\frac{dv(z)}{dz} \tag{4}$$

$$a(z) = -\lambda \cdot \frac{\mu_e}{h} \cdot v(z) \cdot \frac{db(z)}{dz} \tag{5}$$

From Eq. (2) it is seen that the acceleration given by Eq. (5) cannot exceed an upper limit a_0 given by

$$a(z) \le \frac{hk\gamma}{2\pi M} \cdot \frac{I/I_0}{1 + I/I_0} \equiv a_0 \tag{6}$$

This means that the acceleration characterized by a_0 is the physically permitted maximum value in a given condition. According to Eq. (5), however, the mathematical acceleration can be arbitrarily large. This motivates us in the analysis to artificially set the criterion of the physically permitted acceleration given by Eq. (2). It is also important to note that particles cannot follow the local equilibrium velocity given by Eq. (3) if the magnetic gradient is too steep or if the acceleration $a(z)$ exceeds a_0. For the purpose of analytical convenience, all physical parameters were converted to a common physical unit of frequency. This is done because the calculated results can be compared directly with the optical experimental results, and this treatment is compatible with the normalization since the typical velocity obtained by optical measurement is equal approximately to unity in the unit of gigahertz. The physical parameters characterizing laser cooling, that is, the velocity, magnetic field, acceleration, and length, are converted into the frequency space as follows:

$$v, \text{ m/s} \rightarrow \tilde{v} = v/\lambda, \text{ Hz} \tag{7}$$

$$b, \text{ G} \rightarrow \tilde{b} = \mu_e b/h, \text{ Hz} \tag{8}$$

$$a, \text{ m/s}^2 \rightarrow \hat{a} = (L/\lambda^2) \cdot a, \text{ Hz}^2 \tag{9}$$

$$z, \text{ m} \rightarrow \bar{z} = z/L, \text{ dimensionless} \tag{10}$$

where L is the deceleration length of the applied magnetic field. The spatial distribution of the magnetic field can be approximated by the relation:

$$b(z) = b_0[1 - (z/L)] \qquad 0 \le z \le L \tag{11}$$

Writing $\tilde{b}_0 = \mu_e b_0/h$, a_0 in Eq. (6), $a(z)$ in Eq. (5), and $v(z)$ in Eq. (3) are rewritten by

$$\hat{a}_0 = \alpha \cdot L \cdot [I/I_0/(1 + I/I_0)] \tag{12}$$

$$\hat{a}(\bar{z}) = \tilde{b}_0(\delta + \tilde{b}_0 - \tilde{b}_0\bar{z}) \qquad 0 \le \bar{z} \le 1 \tag{13}$$

$$\tilde{v}(\bar{z}) = \delta + \tilde{b}_0 - \tilde{b}_0\bar{z} \le \tilde{C}_0 \qquad 0 \le \bar{z} \le 1 \tag{14}$$

where α is equal to $hk\gamma/2\pi M\lambda^2$, which is a constant 0.39 m^{-1} s^{-2} for the experimental conditions. The critical velocity $\tilde{C}_0$ is defined by the equation

$$\tilde{C}_0 = \hat{a}_0/\tilde{b}_0 \tag{15}$$

From this conversion, the restriction on the local acceleration is now interpreted as a restriction on the maximum velocity permitted for laser cooling. The meaning of the critical velocity is schematically shown in Fig. 14. A particle is decelerated step-by-step at each resonant position where Doppler shift is canceled by Zeeman effect and the detuning of the laser. If the beam velocity is faster than the critical velocity determined by a given experimental condition, the particle passes through the resonant position after a photon absorption–emission process of 2τ. In other words, the velocity of the particle participating in the laser cooling must never exceed the critical velocity. If the particle velocity exceeds the critical velocity, it will not be cooled. Whenever the cooling laser is on, the atomic beam is decelerated to the velocity of δ in the frequency space at the exit of the cooling section as found in Eq. (14). Figure 6 shows a good agreement between δ and the final velocity of the decelerated atomic beam. The critical velocity $\tilde{C}_0$ depends on the magnetic gradient b_0/L and the power of the cooling laser. The inequality in Eq. (14) implies that the laser cooling occurs in a magnetic field yielding a local velocity less than the critical velocity. For $\tilde{C}_0 < \delta$ the inequality is never satisfied at any point of $\bar{z}$. For $\bar{z}$ from $1 - (\tilde{C}_0 - \delta)/\tilde{b}_0$ to 1, the inequality will be satisfied in the region of $\delta \le \tilde{C}_0 \le \delta + \tilde{b}_0$. The inequality is valid throughout the cooling section when $\tilde{C}_0 \ge \delta + \tilde{b}_0$.

Defining W in frequency units, radiative pressure is received by the atoms within the velocity range of δ to $\delta + W$. Figure 15 shows the dependence of deceleration bandwidth in frequency space upon the magnetic strength. The deceleration bandwidth is given by

$$\begin{aligned} W &= \tilde{b}_0 \quad \text{for} \quad 0 \le \tilde{b}_0 \le (\sqrt{\delta^2 + 4\hat{a}_0} - \delta)/2 \\ &= \tilde{C}_0 - \delta \quad \text{for} \quad (\sqrt{\delta^2 + 4\hat{a}_0} - \delta)/2 \le \tilde{b}_0 \le (\hat{a}_0/\delta) \\ &= 0 \quad \text{for} \quad (\hat{a}_0/\delta) \le \tilde{b}_0 \end{aligned} \tag{16}$$

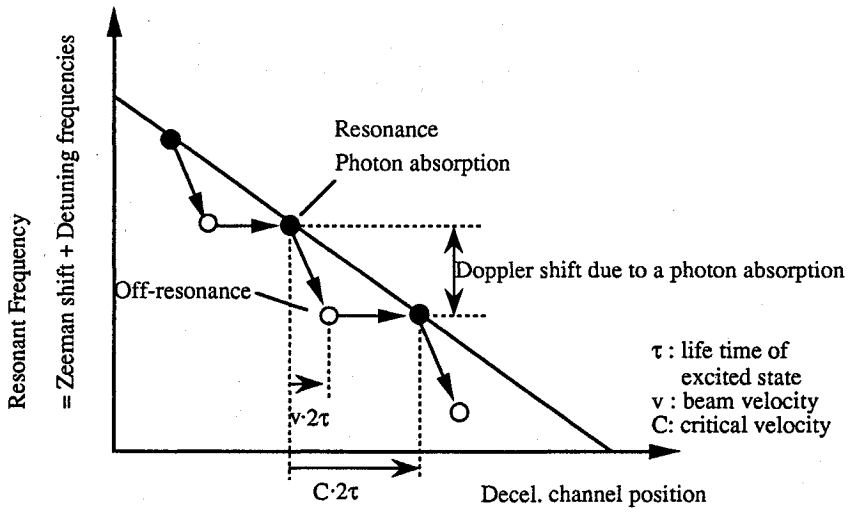

Fig. 14 Meaning of critical velocity.

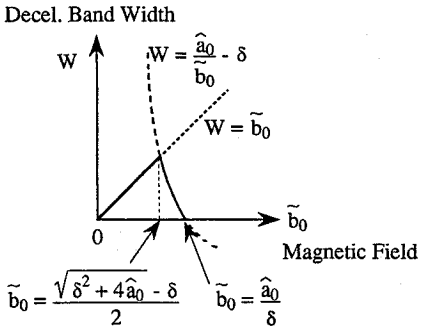

Fig. 15 Relation between deceleration bandwidth and magnetic field.

The bandwidth increases in proportion to the magnetic strength in weak fields but decreases in strong fields. The deceleration bandwidth is closely related to the decelerated number. The points of $\tilde{b}_0 = (\sqrt{\delta^2 + 4\hat{a}_0} - \delta)/2$ and $\tilde{b}_0 = \hat{a}_0/\delta$ are indicated in Fig. 12, where experimental results prove that the decelerated number at the weak magnetic field is larger than that for higher fields.

A numerical analysis was performed assuming that the initial beam distribution is a drifting Maxwellian with a beam velocity of 1 GHz (813 m/s) and a full width of half-maximum (FWHM) of 0.4 GHz (325 m/s). The total area of the distribution is normalized to unity as in the experiments. Using the detuning frequency δ, the bandwidth W, and function $f(v)$, the S_1 is given by

$$S_1 = \int_{\delta}^{\delta+W} f(\tilde{v})\, d\tilde{v} \tag{17}$$

Figure 10 shows the resulting calculated decelerated number as a function of the absolute detuning frequency for the laser-power density 43 mW/cm^2 and deceleration length of 0.4 m used during the experiment. For detuning frequencies less than 0.8 GHz with a maximum magnetic field strength of 100 G, the decelerated number increases with the detuning frequency because the deceleration band shifts to a more populated region in the velocity distribution of the atomic beam. At higher detuning frequencies the decelerated number rapidly drops to zero because of narrowing of the deceleration bandwidth. The decelerated number at 220 G is lower than that at 100 G because the steep magnetic field gradient narrows the deceleration bandwidth and increases the number of free-running particles in the cooling section. The numerical analysis results agree well with the behavior of the experiment.

For a constant magnetic field gradient and a fixed detuning of the cooling laser, the critical velocity depends on I/I_0 as seen in Eq. (14). For a laser power of I/I_0, much less than unity the critical velocity is linearly proportional to the laser power, but saturates as the power grows. As the laser power is lowered, the deceleration bandwidth decreases, raising the number of the free-running species, which are never affected by the radiation pressure. The positive relation of the decelerated number on the laser power in Fig. 13 agrees qualitatively with Eq. (15).

Implications for Antimatter Storage

To relate these results to the antihydrogen storage, the following parameters in frequency units must be nondimensionalized using γ, which characterizes the laser radiation force:

Velocity:

$$\tilde{v} \rightarrow \tilde{v}/\gamma \tag{18}$$

Magnetic field:

$$\tilde{b} \rightarrow \tilde{b}/\gamma \tag{19}$$

Acceleration:

$$\tilde{C} \rightarrow \tilde{C}/\gamma \tag{20}$$

Critical velocity:

$$\tilde{C} \rightarrow \tilde{C}/\gamma \tag{21}$$

Another nondimensional parameter is I/I_0, which is so-called saturation parameter. To keep the similarity between the sim-

Table 1 Comparison between simulation and antimatter factory

Physical parameters	Simulation	Antimatter factory
Laser wavelength	812 nm	122 nm
Laser power	7 mW	26 W
Deceleration channel length	0.4 m	0.4 mm
Magnetic field strength	100 G	1.3 kG
Beam velocity	800 ms^{-1}	1540 ms^{-1}
Detuning frequency	0.8 GHz	10 GHz
Deceleration energy fraction	0.28	0.28
Decelerated particles	5×10^7 cm^{-2} s^{-1}	5×10^7 cm^{-2} s^{-1}

ulation and the flowfield of the antihydrogen, one requires that these five nondimensional values be constant. It is noted that Eq. (18) can be rewritten as $(\gamma/kv)^{-1}$ and these replacements naturally satisfy the previous assumption used in Eq. (2). A decelerated energy fraction is also defined by dividing the lost energy caused by the laser irradiation by the mean kinetic energy of the atomic beam and evaluated as 0.28. The results of the previous translation are shown in Table 1. It is found that in terms of the channel length for the laser cooling, the experimental results simulate the final phase of the deceleration channel of the antihydrogen storage and corresponds to that of only the final 1 mm or less. Nevertheless, the results experimentally confirm the principle and adequacy of applying the laser cooling to the antihydrogen storage. A future antimatter factory, depending on the initial beam velocity of antihydrogen, will require much longer deceleration length of hundreds of meters than that simulated by the experiment. For application to the antimatter propulsion, one requires antihydrogen of 1 mg/yr or 2×10^{13} decelerated particles/s. This simulation using argon is only 0.004% of the required level.

Conclusions

Laser cooling of neutral antihydrogen is a promising technique for antimatter storage. In this work, laser cooling of metastable argon was demonstrated by means of Zeeman tuning to demonstrate the feasibility of the technique for antihydrogen. A decelerated number of 0.12 and recovery factor of 0.65 were obtained with an atomic flux density of 3.1×10^8 cm^{-2} s^{-1}, a peak magnetic field of 100 G, and a laser power of 7 mW. The particle loss mechanisms were identified as diffusion loss and the loss caused by the free running particles. One-dimensional analysis indicated the existence of the free-running particle loss and shows the existence of a critical velocity above which laser cooling is not possible. The critical velocity is dependent on the magnetic gradient and the laser power. The analysis gave the qualitative explanation of the experimental data. By the similarity law of the flowfield, this study simulated the final 1-mm phase of an antihydrogen deceleration channel. The flux decelerated by the laser amounted to 0.004% of the level required for antimatter propulsion (1 mg/yr or 2×10^{13} decelerated particles/s).

For the application to the antimatter storage, it is preferable that both the decelerated number and the recovery factor should be as large as possible for the purpose of the minimum antiparticle loss. The recovery factor obtained in the experiment may not be sufficient, but it can be improved at least theoretically by adding transverse cooling. The decelerated numbers remained small since the criterion of the critical velocity restricted the deceleration bandwidth for our experimental condition. For further improvement of the decelerated number, the laser-cooling parameters, such as velocity, magnetic field strength, deceleration length, and laser-power density, must be adjusted to ensure that the local velocity of the particle never exceeds the critical velocity throughout the deceleration channel.

Acknowledgment

The authors acknowledge the technical advice of H. Katori in the design of the cooling laser and the diagnostic instruments.

References

[1]Forward, R. L., "Antiproton Annihilation Propulsion," Air Force Rocket Propulsion Lab., AD-A160-734, Sept. 1985.

[2]Howe, S. D., and Metzger, S. D., "Antiproton-Based Propulsion Concepts and the Potential Impact on a Manned Mars Mission," *Journal of Propulsion and Power*, Vol. 5, No. 3, 1985, pp. 295–300.

[3]Vulpetti, G., "Multiple Propulsion Concept for Interstellar Flight: General Theory and Basic Results," *Journal of the British Interplanetary Society*, Vol. 43, No. 12, 1990, pp. 537–550.

[4]Massier, P. F., "The Need for Expanded Exploration of Matter-Antimatter Annihilation for Propulsion Application," *Journal of the British Interplanetary Society*, Vol. 35, No. 9, 1982, pp. 387–390.

[5]Vulpetti, G., "Relativistic Astrodynamics: The Problem of Payload Optimization in a Two-Star Exploration Flight with an Intermediate Powered Swing-By," *Journal of the British Interplanetary Society*, Vol. 37, No. 9, 1984, pp. 515–521.

[6]Nordley, G. D., "Application of Antimatter-Electric Power to Interstellar Propulsion," *Journal of the British Interplanetary Society*, Vol. 43, No. 6, 1990, pp. 241–258.

[7]Vulpetti, G., and Pecchioli, M., "Consideration About the Specific Impulse of an Antimatter-Based Thermal Engine," *Journal of Propulsion and Power*, Vol. 5, No. 5, 1989, pp. 591–595.

[8]Cassenti, B. N., "Antimatter Propulsion for OTV Applications," AIAA Paper 84-1485, July 1989.

[9]LaPointe, M. R., "Antiproton Powered Propulsion with Magnetically Confined Plasma Engines," *Journal of Propulsion and Power*, Vol. 7, No. 5, 1991, pp. 749–759.

[10]Morgan, D. L., Jr., "Concepts for the Design of an Antimatter Annihilation Rocket," *Journal of the British Interplanetary Society*, Vol. 35, No. 9, 1982, pp. 405–412.

[11]Wickman, J. H., "Technology Assessment of Photon Propulsion: How Close Are We?," AIAA Paper 81-1532, July 1981.

[12]Forward, R. L., Cassenti, B. N., and Miller, D., "Cost Comparison of Chemical and Antihydrogen Propulsion Systems for High ΔV Missions," AIAA Paper 85-1455, July 1985.

[13]People, J., "The Fermilab Antiproton Source," *IEEE Transactions on Nuclear Science*, Vol. NS-30, No. 4, 1983, pp. 1970–1975.

[14]Chirikov, B. V., Tayurski, V. A., Möhring, H. J., Ranft, J., and Schirrmeister, V., "Optimization of Antiproton Fluxes from Target Using Hadron Cascade Model," *Nuclear Instruments and Methods*, Vol. 144, No. 2, 1977, pp. 129–139.

[15]Hojvat, C., and Van Ginneken, A., "Calculation of Antiproton Yields for the Fermilab Antiproton Source," *Nuclear Instruments and Methods*, Vol. 206, No. 1, 1983, pp. 67–83.

[16]Neumann, R., Poth, H., Winnacher, A., and Wolf, A., "Laser-Enhanced Electron-Ion Capture and Antihydrogen Formation," *Zeitschrift für Physik A: Atoms and Nuclei*, Vol. 313, No. 4, 1983, pp. 253–262.

[17]Phillips, W. D., Prodan, J. V., and Metcalf, H. J., "Laser Cooling and Electromagnetic Trapping of Neutral Atoms," *Journal of the Optical Society of America B*, Vol. 2, No. 11, 1985, pp. 1751–1767.

[18]Balykin, V. I., Letokhov, V. S., Minogin, V. G., Rozhdestvensky, Y. V., and Sidorov, A. I., "Radiative Collimation of Atomic Beams Through Two-Dimensional Cooling of Atoms by Laser-Radiation Pressure," *Journal of the Optical Society of America B*, Vol. 2, No. 11, 1985, pp. 1776–1783.

[19]Ertmer, W., Blatt, R., Hall, J. L., and Zhu, M., "Laser Manipulation of Atomic Beam Velocities: Demonstration of Stopped Atoms and Velocity Reversal," *Physical Review Letters*, Vol. 54, No. 10, 1985, pp. 996–999.

[20]Nellesen, J., Müller, J. H., Sengstock, K., and Ertner, W., "Large-Angle Beam Deflection of a Laser-Cooled Sodium Beam," *Journal of the Optical Society of America B*, Vol. 6, No. 11, 1989, pp. 2149–2154.

[21]Shimizu, F., Shimizu, K., and Takuma, H., "Laser Cooling of a Neon Atomic Beam in Metastable States," *Japanese Journal of Applied Physics*, Vol. 26, No. 11, 1987, pp. L1847–L1849.

[22]Watts, R. N., and Wieman, C. E., "Manipulating Atomic Velocities Using Diode Laser," *Optics Letters*, Vol. 11, No. 5, 1986, pp. 291–293.

[23]Sesko, D., Fan, C. G., and Wieman, C. E., "Production of a Cold Atomic Vapor Using Diode-Laser Cooling," *Journal of the Optical Society of America B*, Vol. 5, No. 6, 1988, pp. 1225–1227.

[24]Katori, H., and Shimizu, F., "Laser Cooling and Trapping of Argon and Krypton Using Diode Lasers," *Japanese Journal of Applied Physics*, Vol. 29, No. 11, 1990, pp. L2124–L2126.

[25]Ciocci, F., Dattoli, G., De Angelis, A., Faatz, B., Garosi, G., Giannessi, L., Ottaviani, P. L., and Torre, A., "Design Considerations on a High Power VUV FEL," *IEEE Journal of Quantum Electronics*, Vol. 31, No. 7, 1995.

[26]Minogin, V. G., *Laser Light Pressure on Atoms*, Gordon and Breach, New York, 1987, pp. 23–26.